X-ray diffraction and magnetic measurements of itinerant electron magnetism in the $Y_3Ni_{13-x}Co_xB_2$ system

N. Plugaru,* J. Rubín, and J. Bartolomé
Instituto de Ciencia de Materiales de Aragón-CSIC, Universidad de Zaragoza, 50009 Zaragoza, Spain

V. Pop†
Faculty of Physics, Babes-Bolyai University, 400084, Cluj-Napoca, Romania
(Received 21 June 2004; revised manuscript received 28 October 2004; published 31 January 2005)

The crystallographic and magnetic properties of the $Y_3Ni_{13-x}Co_xB_2$ series of compounds, with the $Nd_3Ni_{13}B_2$-type structure and $x \leqslant 5$, were investigated by powder x-ray diffraction and magnetic measurements. The susceptibility and magnetization data show that $Y_3Ni_{13}B_2$ is a weak itinerant antiferromagnet with a Néel temperature $T_N = 68$ K. A weak ferromagnetic component appears at T_N, suggesting uncompensated antiferromagnetic structure. The compounds with $x = 0.5$ and 1, also order antiferromagnetically, with $T_N = 94$ and 106 K, respectively. The intrinsic weak ferromagnetic component increases with the cobalt content and a field-induced transition, from the antiferromagnetic state to a ferromagnetic state, is observed at the critical transition fields 5.6 and 1.6 T, at 5 K for $x = 0.5$ and 1, respectively. A heterogeneous ferromagnetic state and in-plane magnetic anisotropy are determined for the compounds in the $2 \leqslant x \leqslant 5$ composition range. The Curie temperature and spontaneous magnetization increase linearly with the cobalt content. Based on the experimental data, the *T-x* phase diagram is constructed for $x \leqslant 5$. The effect of spin fluctuations is highlighted in the nickel-rich compounds in the 3:13:2 and related systems.

DOI: 10.1103/PhysRevB.71.024433 PACS number(s): 75.30.Cr, 75.30.Et, 75.30.Gw

I. INTRODUCTION

The compounds pertaining to the series formally denoted by $R_{m+n}T_{5m+3n}+B_{2n}$ (with space group symmetry $P6/mmm$) and T=Co or Ni, crystallize in layered structures which consist of systematically stacked m $CaCu_5$-type layers and n $CeCo_3B_2$-type layers.[1] Whereas the cobalt-based compounds have received a particular interest due to the excellent hard magnetic properties of the RCo_5 ($m=1$ and $n=0$) and related R_2Co_{17} phases,[2–4] the Ni-based compounds have mainly been studied for exhibiting various manifestations of weak itinerant ferromagnetism, crystal electrostatic field effects, and spin fluctuations.[5] Thus, a giant magnetocrystalline anisotropy and a strong crystal field effect on the magnetic interactions have been determined in RNi_5 compounds[6,7] and even an enhancement of these in the RNi_4B series ($m=1$ and $n=1$) is supported by the magnetic data.[8] YNi_4B has thoroughly been studied to a large extent because of its presumed superconducting behavior, which subsequently has been attributed to the occurrence of the YNi_2B_2C phase.[9,10] The development of large intrinsic coercivity at low temperature in $R(Ni,Co)_5$ in the intermediary composition range has been explained by the coexistence of high- and low-Co magnetic moments in the metallic compounds;[11–13] moreover, the observation of metamagnetic transitions in $R(Co,Ni)_5$ where R=Th[14] or Ce[15,16] as well as theoretical results and high magnetic field data for the $Y(Co,Ni)_5$ compounds[17,18] have been associated with the presence of both high and low Co moment states in these systems.

Proceeding further by increasing m in the $R_{m+n}T_{5m+3n}B_{2n}$ series, one obtains the $R_3T_{13}B_2$ stoichiometry (for $m=2$ and $n=1$); the $Nd_3Ni_{13}B_2$-type crystal structure was analyzed in the early 1980s.[19–21] The unit cell, drawn in Fig. 1, consists of two 1:5 slabs stacked between 1:3:2 slabs. There are three types of layers: (i) *T*-only containing layers, $T(3g)$ and $T(6i)$, (ii) $R(2e)-T(4h)$ layers, and (iii) $R(1a)-B(2c)$ layers. The first order coordination at the crystallographically inequivalent lattice sites is given in Table I. A literature search on the magnetic properties of $R_3Ni_{13}B_2$ yielded that $Y_3Ni_{13}B_2$ is reported to order magnetically below a Curie temperature $T_C=65$ K, inferred from the temperature dependence of ac susceptibility data in the $Y_{1+\delta}Ni_{4-x}B_{1+x}$ series.[9] This behavior would not be singular: on the Y-Ni-B phase diagram[21] the magnetically ordered $Y_3Ni_{13}B_2$ lies between YNi_5 and YNi_4B, both showing paramagnetic behavior,[22] similarly to the case of the weak ferromagnetic (WF) Y_2Ni_7 and YNi_3, which are situated between the paramagnetic YNi_5 and YNi_2.[7] In order to account for the resurgence of magnetism

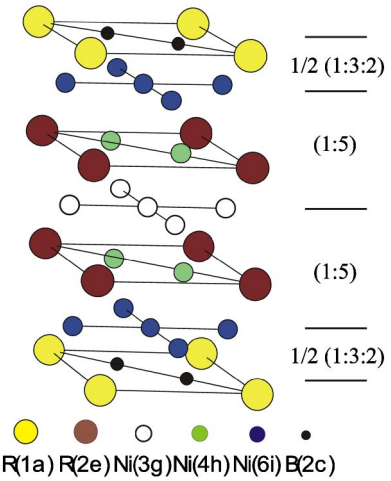

FIG. 1. The $Nd_3Ni_{13}B_2$-type unit cell (S.G. $P6/mmm$).

TABLE I. First-order coordination at the inequivalent lattice sites in the $Nd_3Ni_{13}B_2$-type structure.

Atom	Ni(6*i*)	Ni(3*g*)	Ni(4*h*)	*R*(1*a*)	*R*(2*e*)	B(2*c*)
Ni(6*i*)	5		2	2	2	2
Ni(3*g*)		4	4		4	
Ni(4*h*)	3	3	3		3	
R(1*a*)	12				2	6
R(2*e*)	6	6	6	1	1	
B(2*c*)	6			3		

in $Y_3Ni_{13}B_2$ it was proposed that, on the grounds of similar crystallographic environments of Ni atoms in $Y_3Ni_{13}B_2$, YNi_5, and YNi_4B, the Fermi level is situated for both YNi_5 and YNi_4B in minima of the density of states, but in a maximum for $Y_3Ni_{13}B_2$, where the Stoner criterion is fulfilled and magnetic order occurs.[9] To our knowledge, there is no other account on the magnetic properties of $Y_3Ni_{13}B_2$ compound, hitherto.

Recently, under the prospect of synthesizing Co-rich $R_3T_{13}B_2$ alloys with the $Nd_3Ni_{13}B_2$ structure and potential permanent magnetic applications, the preparation of the $Nd_3Co_{13}B_2$ compound with the $Nd_3Ni_{13}B_2$ structure has been reported.[23,24] A Curie temperature of 710 K, a saturation magnetization of 20.8 μ_B/f.u. at 4.2 K, and an anisotropy field $H_A=180$ kOe at 5 K, with the easy magnetization direction (EMD) confined within the basal plane below a spin reorientation temperature at $T_{SR}=370$ K were determined for this compound. Studies of phase equilibria in *R*-Co-B systems where *R*=Pr,[25] Gd,[26] and Sm[27] revealed the crystallization of the $R_3Co_{13}B_2$ compounds with the $Nd_3Ni_{13}B_2$ structure; however, it was found that the preparation of single phase $R_3Co_{13}B_2$ is rather difficult because of the concomitant formation of the RCo_4B and RCo_5 secondary phases.

Therefore, the interest in the description of itinerant electron magnetism of the (Co,Ni) sublattice in new members of the $R_{m+n}T_{5m+3n}B_{2n}$ series, the lack of detailed data on the magnetic properties of $R_3Ni_{13}B_2$, as well as a continuous search for new phases with potential for technical applications have motivated the present research work. Herein, we report on the synthesis, crystal structure and magnetic properties of the $Y_3Ni_{13-x}Co_xB_2$ compounds. The complex magnetic state of the 3*d* electron system for low Co content ($x \leqslant 1.0$) and its evolution to ferromagnetism when *x* increases are investigated. A magnetic phase diagram in *T*-*x* coordinates is proposed for $x \leqslant 5.0$ and the magnetic behavior of the 3*d* sublattice in $Y_3(Ni,Co)_{13}B_2$ and related systems is discussed.

II. EXPERIMENTAL

Batches of alloys with the nominal compositions $Y_3Ni_{13-x}Co_xB_2$, where $x=0,0.5,1,2,3,4,5,6,8,10$, and 13, were prepared by induction melting, under Ar atmosphere. Pure elements (3*N* yttrium, nickel and cobalt and 2*N*7 polycrystalline boron) in stoichiometric amounts, but with a 1.5 wt.% yttrium excess, were used as starting materials. The buttons were sealed in silica tubes under Ar gas and annealed at temperatures between 950–1323 K for two to six weeks, then quenched. The phase content and the crystal structure were investigated by powder x-ray diffraction using a rotating-anode Rigaku diffractometer, with Cu-K_α radiation, at room temperature (RT). In order to reduce the texture, the samples were finely ground and mixed with CAB-OSIL M-5 amorphous powder from Fluka. The structural parameters were derived by Rietveld refinement of the patterns using the FullProf.98 Version 0.2 software.[28] X-ray diffraction on random and field-oriented samples, with $2 \leqslant x \leqslant 5$, was used to determine the EMD, in a temperature domain just below the Curie point. The intensity analysis was carried out on pairs of lines with (*hkl*): (103) and (004), (200) and (005), and (203) and (006). The powders were aligned in a Sm-Co permanent magnet circuit, cooled down to the liquid nitrogen temperature, where the samples are ferromagnetic (*F*); then, the ensemble was left to warm up to RT, the powders retaining the texture induced by the magnetic field below T_C.

Scanning electron microscopy (SEM) and elemental microprobe analysis (EDAX) were additionally used for the identification of the secondary phases. Thermomagnetic curves were measured between 300–1150 K by using a

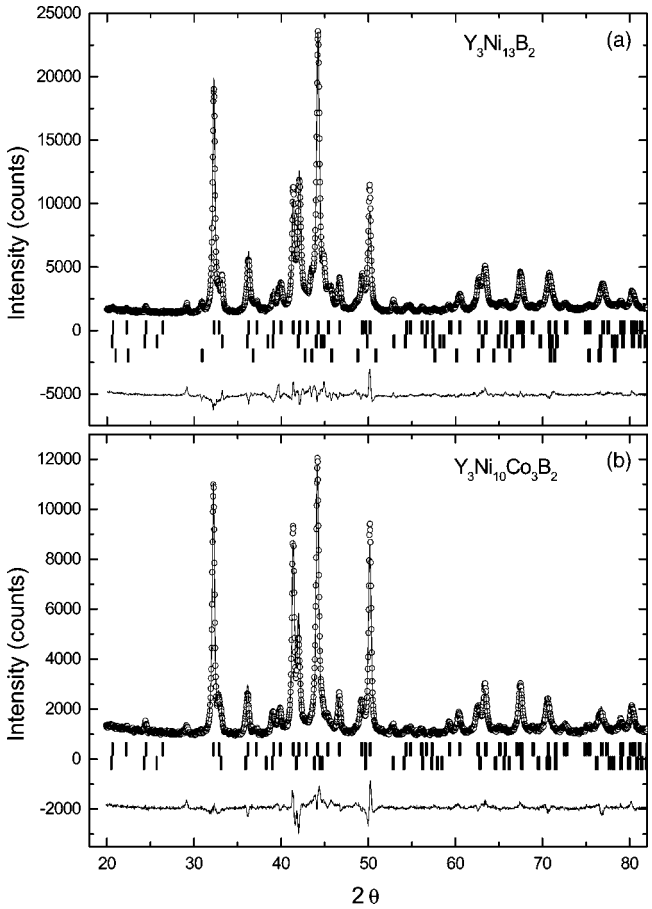

FIG. 2. Experimental, calculated and difference x-ray diffraction patterns of the $Y_3Ni_{13}B_2$ (a) and $Y_3Ni_{10}Co_3B_2$ (b) compounds. The bars marking the reflections correspond to the phases 3:13:2 (top), 1:4:1 (middle), and 1:5 (bottom).

TABLE II. Phase content (wt.%) of various phases in the $Y_3Ni_{13-x}Co_xB_2$ samples with $x \leqslant 5$.

x, Co	3:13:2	1:4:1	1:5
0	89.4(1.4)	8.5(2)	1.7(1)
0.5	88.6(1.8)	7.1(2)	2.9(1)
1	88.4(2.0)	8.4(3)	1.9(2)
2	90.5(1.4)	8.1(2)	0.6(1)
3	95.3(1.2)	3.8(2)	
4	93.6(1.1)	5.2(1)	0.4(1)
5	85.0(1.4)	11.2(3)	2.8(2)

Faraday-type balance, in order to probe the occurrence of ferromagnetic impurities. As a result of the sample quality investigations, discussed below, only the compounds with $x \leqslant 5$ were selected for subsequent magnetic measurements.

The magnetization and susceptibility measurements were performed using a superconducting quantum interference device (SQUID) magnetometer model MPMS from Quantum Design, in dc applied field H_0 up to 5 T, in the temperature range 1.8–300 K. The measurements were carried out on powder samples for all compositions, and also on various specimens of platelet-shaped crystals and stacked crystals detached from the bulk, for $x \leqslant 1$. In the latter case, the plane of the platelets was assessed by Laue diffraction to be parallel to the crystallographic (001) plane, which allowed us to orient the samples with the c axis parallel as well as perpendicular to the direction of the applied field H_0. The magnetization of the compounds with $x=0$ and 0.5 was also measured in a vibrating sample magnetometer in field up to 10 T, at 2 and 5 K. The analysis of the $M(H)$ curves and the correction brought to the spontaneous magnetization values M_S due to the occurrence of ferromagnetic impurities, will be discussed for each compound separately. The temperature dependence of the remanent magnetization was measured on stacked crystals, for $x=0$ and 0.5, after the application of a magnetizing field of 5 T at 5 K. Hysteresis loops were also

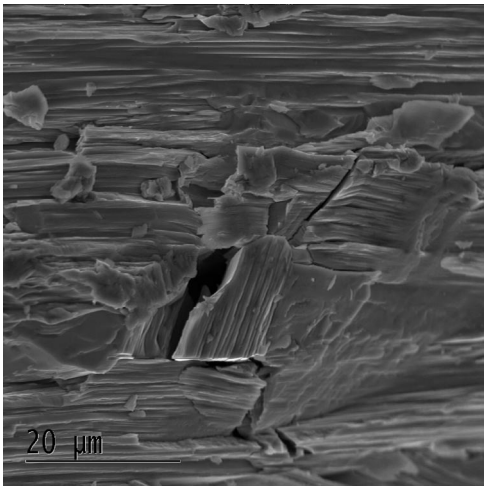

FIG. 3. Secondary electrons SEM image showing the microstructure of the $Y_3Ni_{13}B_2$ sample.

TABLE III. Lattice constants a and c, their ratio, special fractional atomic positions z, unit cell volume V_{UC}, overall isotropic temperature factor B_{ov}, Bragg R factor R_B, and interatomic distances d.

Parameter	$Y_3Ni_{13}B_2$	$Y_3Ni_{12.5}Co_{0.5}B_2$	$Y_3Ni_{12}CoB_2$	$Y_3Ni_{11}Co_2B_2$	$Y_3Ni_{10}Co_3B_2$	$Y_3Ni_9Co_4B_2$	$Y_3Ni_8Co_5B_2$
a (Å)	4.9579(1)	4.9566(2)	4.9585(2)	4.9584(3)	4.9597(2)	4.9649(2)	4.9661(2)
c (Å)	10.9141(3)	10.9072(3)	10.9059(3)	10.9013(6)	10.8930(3)	10.8933(3)	10.8867(3)
c/a	2.201	2.201	2.199	2.199	2.196	2.194	2.192
z,6i	0.1338(1)	0.1348(2)	0.1347(2)	0.1345(2)	0.1346(2)	0.1355(2)	0.1365(3)
z,4h	0.3186(2)	0.3174(4)	0.3180(4)	0.3176(3)	0.3188(3)	0.3187(4)	0.3182(5)
z,2e	0.3278(2)	0.3292(3)	0.3282(4)	0.3274(3)	0.3260(3)	0.3250(4)	0.3265(4)
V_{UC} (Å^3)	232.3	232.1	232.2	232.1	232.1	232.5	232.5
B_{ov} (Å^2)	0.33(8)	0.36(7)	0.35(9)	0.41(8)	0.42(7)	0.49(6)	0.31(6)
R_B	5.56	8.15	9.08	7.69	6.77	5.77	9.27
$d_{6i\text{-}6i}$(Å)	2.48	2.48	2.48	2.48	2.48	2.48	2.48
	2.94	2.94	2.94	2.93	2.93	2.95	2.97
$d_{6i\text{-}4h}$ (Å)	2.47	2.45	2.46	2.46	2.46	2.46	2.44
$d_{6i\text{-}2e}$ (Å)	3.25	3.26	3.26	3.25	3.24	3.23	3.23
$d_{6i\text{-}2c}$ (Å)	2.05	2.05	2.05	2.05	2.05	2.06	2.06
$d_{6i\text{-}1a}$ (Å)	2.88	2.88	2.88	2.88	2.88	2.89	2.89
$d_{4h\text{-}4h}$ (Å)	2.86	2.86	2.86	2.86	2.86	2.87	2.87
$d_{4h\text{-}3g}$ (Å)	2.43	2.45	2.45	2.45	2.44	2.44	2.44
$d_{4h\text{-}2e}$ (Å)	2.86	2.86	2.87	2.86	2.86	2.87	2.87
$d_{3g\text{-}3g}$ (Å)	2.48	2.48	2.48	2.48	2.48	2.48	2.48
$d_{3g\text{-}2e}$ (Å)	3.11	3.10	3.11	3.11	3.12	3.13	3.12
$d_{2c\text{-}1a}$ (Å)	2.86	2.86	2.86	2.86	2.86	2.87	2.87

measured at 5 K for the samples with $2 \leqslant x \leqslant 5$, on coarse powders embedded in highly viscous silicon grease, thus preventing the rotation of the grains in a high magnetic field. The temperature dependence of the ac susceptibility χ_{ac} was measured with an ac excitation field of 3.5 Oe and 90 Hz.

III. RESULTS

A. Phase formation and crystal structure parameters

The 3:13:2 phase with the $Nd_3Ni_{13}B_2$ structure was identified in the x-ray diffraction patterns of the samples annealed between 973–1050 K, for all the composition range; however, it was found in a fraction of at least 85 wt.% only in the samples with a cobalt content $x \leqslant 5$. The $Y_3Co_{13}B_2$ compound, for which we have determined the lattice constants $a = 5.006(0)$ Å and $c = 10.851(1)$Å, appeared in a fraction of about 50 wt.% in the batch with $x = 13$. Some representative, experimental and calculated, diffraction patterns are plotted in Figs. 2(a) and 2(b). The patterns of the samples with amorphous powder addition still reveal a (00*k*) texture, as proven by the comparison with the calculated model for a randomly oriented powder. From the analysis of the x-ray diffraction and thermomagnetic data, the samples investigated in the present study were selected such as to contain minimum amounts of the $Y(Ni,Co)_4B$ and $Y(Ni,Co)_5$, and also no traces of $Y_2(Ni,Co)_{17}$, or YNi_2B_2C, or nickel borides. The phase contents of the samples, as given by the refinements, are listed in Table II. Small amounts (<1 wt.%) of yttrium oxide, revealed by its 100% (222) reflection at $2\theta \approx 29.1°$ were also detected (but not included in the plots in Fig. 2). Because of the presence of the secondary phases one should expect small deviations from the nominal stoichiometries of the compounds. A secondary electron SEM image, representative for the microstructure of a $Y_3Ni_{13}B_2$ sample in this study, is shown in Fig. 3; the microstructure consists of conglomerates of rather large, platelet-shaped crystallites. No phase contrast, expected to be reduced due to the close Y to Ni atom ratios (0.23, 0.25, and 0.20 for the 3:13:2, 1:4:1, and 1:5 phases, respectively), could be evidenced in the backscattered electron images of the compounds, to allow the identification of the secondary phases. Actually, the crystallites show smooth and clean surfaces. We suggest that the 1:4:1 and 1:5 secondary phases, in the limit of the small fractions observed by x-ray diffraction of the superstructured $Nd_3Ni_{13}B_2$-type cell, mainly represent 3:13:2 defect cells at the grain boundaries.

The structural parameters are listed in Table III. The lattice constants of $Y_3Ni_{13}B_2$, in the present work, are somewhat larger (by 0.2%) than the values $a = 4.942(3)$Å and $c = 10.886(11)$ Å reported in Refs. 19–21. The YNi_5 slab in the $Y_3Ni_{13}B_2$ cell (Fig. 1) has the lattice constants $a_{1:5}^{3:13:2} = 4.95$ Å and $c_{1:5}^{3:13:2} = 3.98$ Å, which are close to those of the YNi_5 slab in the YNi_4B cell, i.e., $a_{1:5}^{1:4:1} = 4.96$ Å and $c_{1:5}^{1:4:1} = 3.97$ Å; the *a* constant in $Y_3Ni_{13}B_2$ is by 1.4% larger than that of the pure YNi_5 [$a_{1:5} = 4.88$ Å and $c_{1:5} = 3.97$ Å (Ref. 29)]. The other building block YNi_3B_2, which does not form as a separate phase, has the same *c* constant in the 3:13:2 and 1:4:1 phases $c_{1:3:2} = 2.94$ Å.

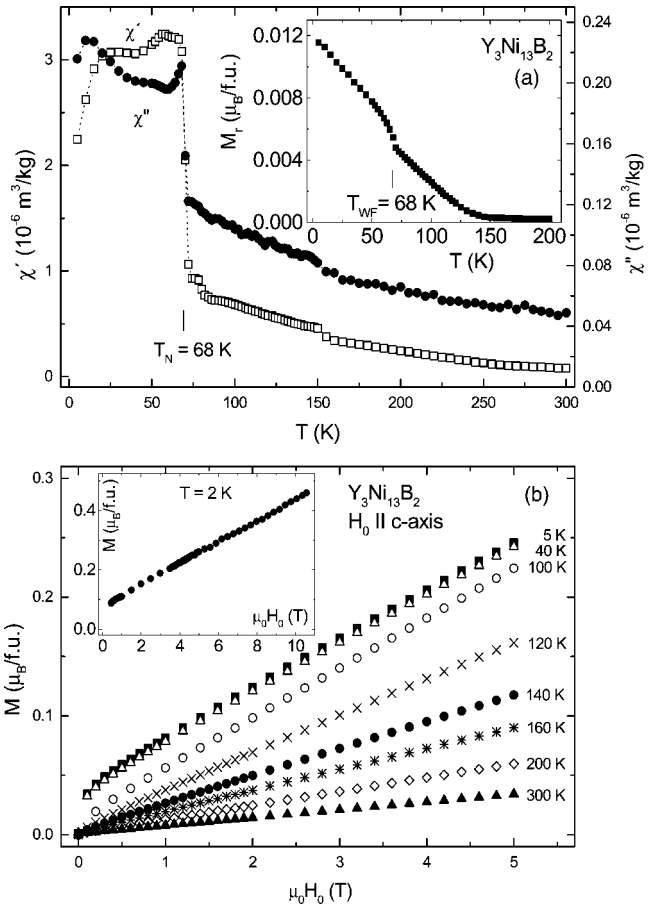

FIG. 4. The temperature dependence of the ac susceptibility (a) and the magnetization isotherms with the applied field parallel to the *c* axis of $Y_3Ni_{13}B_2$ (b). Inset in (a): the temperature dependence of the remanent magnetization. Inset in (b): the $M(H)$ curve in a field up to 10 T, at 2 K, for $H_0 \| c$ axis.

We note that when *x* increases from 0 to 5, *c* decreases by 0.2% while *a* increases by 0.2%, accounting for a monotonic decrease of the c/a ratio from 2.202 in $Y_3Ni_{13}B_2$ to 2.192 in $Y_3Ni_8Co_5B_2$ and to 2.168 in $Y_3Co_{13}B_2$. Previously, in the $Y(Co,Ni)_5$ series, such a composition dependence of the lattice constants was attributed to the Co 3*g* sites preferential occupation;[30] also, recent *ab initio* calculations of the binding energies in $Y(Co,T)_5$ and $Y(Ni,T)_5$ support the Co 3*g* site and Ni 2*c* site preferential occupations.[31] The 2*c* and 3*g* sites in the $CaCu_5$ structure are related to the (2*c*,4*h*) and (3*g*,6*i*) sites, respectively, in the $Nd_3Ni_{13}B_2$ structure, and the 2*c* sites in the latter are filled by B atoms;[1] having in view that the Co substitution for Ni leads to similar structural effects in the $Y(Co,Ni)_5$ and $Y_3(Ni,Co)_{13}B_2$ series, one can presume, by analogy, that Co preferentially occupies the 6*i* and 3*g* sites in the $Y_3(Ni,Co)_{13}B_2$ compounds, for $x \leqslant 5$. The values of the lattice constants in the $Y_3Ni_{13-x}Co_xB_2$ series (with $x \leqslant 5$) linearly extrapolate well to the corresponding quantities determined for $Y_3Co_{13}B_2$. The unit cell volume shows the trend to increase and a lattice expansion of about 2.3% is determined for the series end Co compound ($x = 13$) with respect to the Ni one ($x = 0$).

TABLE IV. The Néel temperature T_N, the temperature of the onset of the weak ferromagnetic component T_{WF}, the magnetization M, and the superimposed susceptibility χ_0 at 5 K and 5 T for $x=0$ and 1 and at 2 K and 10 T for $x=0.5$, the paramagnetic temperature θ_p and the effective moment p_{eff} in the $Y_3Ni_{13-x}Co_xB_2$ compounds.

x,Co	T_N (±2 K)	T_{WF} (±2 K)	$M_{\parallel}$ (μ_B/f.u.)	$\chi_{0,\parallel}$ (10^{-6} m^3/kg)	$M_{\perp}$ (μ_B/f.u.)	$\chi_{0,\perp}$ (10^{-6} m^3/kg)	θ_p (±2 K)	p_{eff} (μ_B/3d at.)
0	68	68	0.25	0.26	0.29	0.30	76	0.71
0.5	94	86	1.08	0.07	0.96	0.13	76	1.16
1.0	106	92	1.56	0.38	1.22	0.78	79	1.67

B. Magnetic properties

1. $Y_3Ni_{13}B_2$

The temperature dependence of the ac susceptibility and the magnetization isotherms of a sample of stacked crystallites of $Y_3Ni_{13}B_2$ are shown in Figs. 4(a) and 4(b). On lowering the temperature, the susceptibility displays a sharp increase at 68±2 K, indicating the occurrence of a transition from the paramagnetic to the magnetically ordered state. Since the value of the real part of the ac susceptibility at the transition temperature $\chi'=3.19\times10^{-6}$ m^3/kg is by two orders of magnitude smaller than $1/(N_D\rho)$ (where N_D is the demagnetizing coefficient, $N_D=0.55$ and 0.34, for the applied field parallel and perpendicular to the c axis, respectively, and ρ is the x-ray density $\rho=7520$ kg/m^3) expected for a ferromagnetic transition, the state below the transition may be antiferromagnetic (AF), albeit with a weak ferromagnetic component evidenced by the mentioned abrupt jump in χ' and the concomitant one in χ''. Below T_N, χ' shows a plateau until 20 K, where there is a rapid decrease, and χ'' rises and decreases in a similar way to χ'. These phenomena are due to the dynamic character of the ac susceptibility. As soon as the weak ferromagnetism sets on below T_N there appear magnetic domains. The mobility of the domain walls that separate them has a characteristic relaxation time τ; when $\tau\omega_{exp}<1$, where ω_{exp} is the frequency of the ac field, one observes the equilibrium or isothermal χ' characterized by a high value that is maintained while the temperature is reduced until the condition $\tau\omega_{exp}=1$ is approached, then χ' decreases towards the lower, adiabatic value, as observed.

The magnetization curves, shown in Fig. 4(b) at several temperatures for an applied field up to 5 T and in the inset in Fig. 4(b) at 2 K for a field up to 10 T, are linear at all temperatures except at low fields ($\mu_0H_0<0.4$ T), where a small spontaneous magnetization is observed below ~80 K. The values of the magnetization and the superimposed susceptibility χ_0 at 5 K and field of 5 T applied parallel and perpendicular to the c axis of a stacked crystal sample are given in Table IV. The spontaneous magnetization in $Y_3Ni_{13}B_2$ is much smaller than the values reported for ferromagnetic (F) Y-Ni compounds, whereas the superimposed susceptibility is within the same range of values (see Table V).

The temperature dependence of the differential susceptibility at $\mu_0H_0=0.6$ T, plotted in Fig. 5, shows a cusp at about 75 K, which is characteristic of an antiferromagnetic transition and supports that $Y_3Ni_{13}B_2$ orders antiferromagnetically. The maximum value of $\chi_{diff}(T_N)$ is three orders of magnitude smaller than the reciprocal of the demagnetizing factor. The Néel temperature $T_N=68\pm2$ K is that of the largest slope below the cusp,[36] which coincides with the sharp increase in the ac susceptibility. On the other hand, the anomaly in χ is

TABLE V. The Curie temperature T_C, spontaneous magnetization M_s, superimposed susceptibility χ_0, and effective magnetic moment p_{eff}, of ferromagnetic Y-Ni compounds.

Compound	T_C (K)	M_s (μ_B/Ni at.)	χ_0 ($\times10^{-6}$ m^3/kg)	P_{eff} (μ_B/Ni at.)	Reference
Y_2Ni_{17}	149	0.27 (1.5 K)	0.12	1.41	32
Y_2Ni_{16}	142	0.19 (0 K)	0.13		32
Y_2Ni_{15}	119	0.15 (0 K)	0.36	1.35	32
Y_2Ni_7	60	0.061 (4.2 K)			33
Y_2Ni_7	52	0.033 (4.2 K)		0.63	34
$Y_2Ni_{6.9}$	52	0.047 (4.2 K)		0.73	34
$Y_2Ni_{6.8}$	60	0.064 (4.2 K)		0.79	34
$YNi_{2.9}$	32	0.047 (4.2 K)		0.69	34
YNi_3	30	0.04 (4.2 K)	0.11	0.70	35

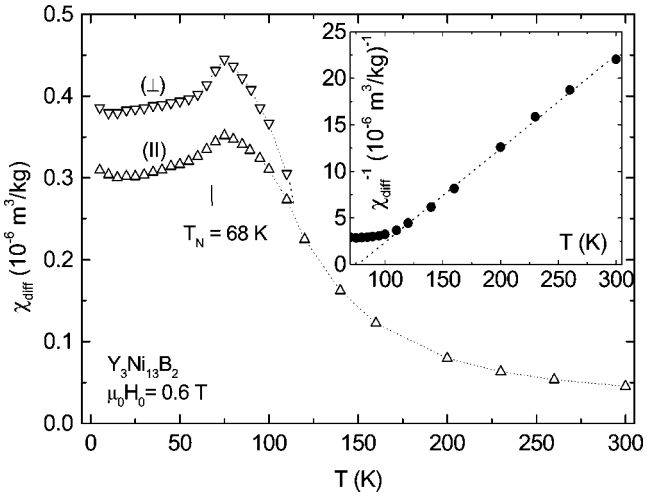

FIG. 5. The temperature dependence of the parallel and perpendicular differential susceptibility of a stacked crystals sample of $Y_3Ni_{13}B_2$, at $\mu_0H_0=0.6$ T. Inset: the temperature dependence of the reciprocal susceptibility.

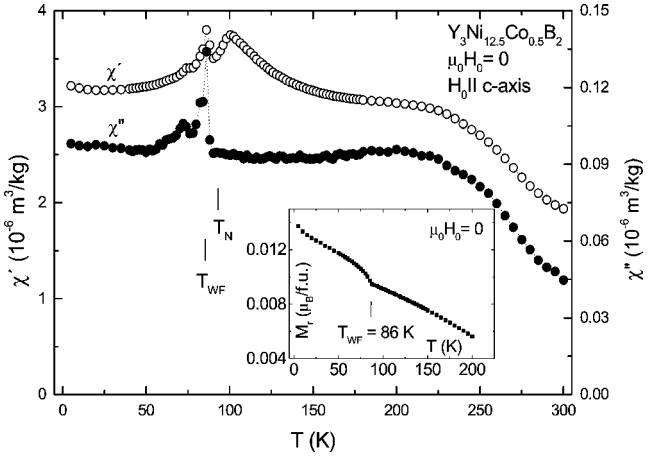

FIG. 6. The temperature dependence of the ac susceptibility of $Y_3Ni_{12.5}Co_{0.5}B_2$. Inset: the temperature dependence of the remanent magnetization.

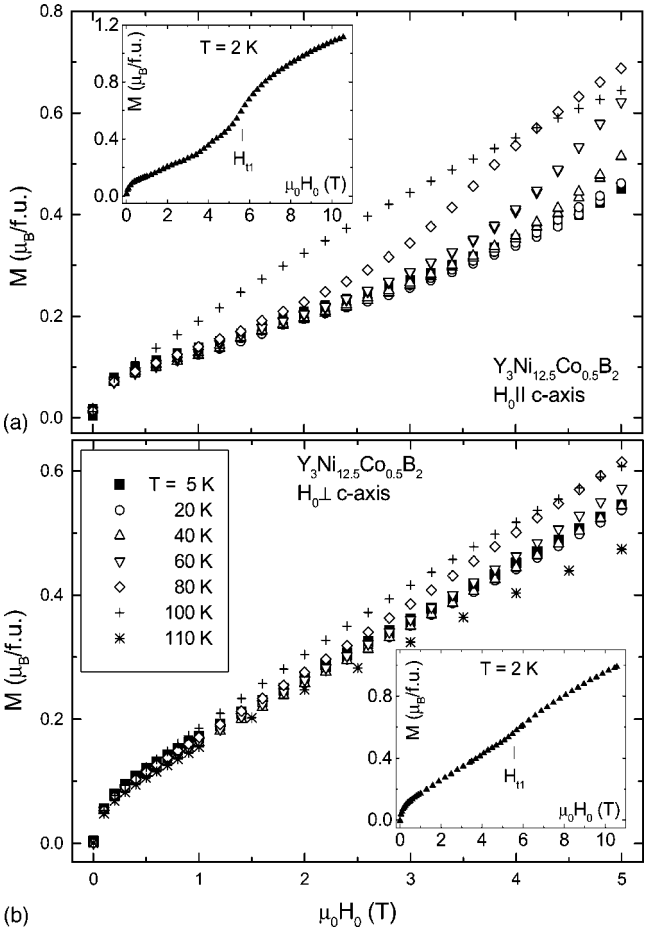

FIG. 7. The magnetization isotherms of the $Y_3Ni_{12.5}Co_{0.5}B_2$ compound in field up to 5 T and various temperatures $T \leqslant 110$ K, with $H_0 \| c$ axis (a) and $H_0 \perp c$ axis (b). Insets in (a) and (b): the corresponding $M(H)$ curves in field up to 10 T at 2 K.

now quenched since the weak ferromagnetic component is saturated at $\mu_0 H_0 = 0.6$ T. Below T_N, the temperature dependence of χ_{diff} for the two orientation of the applied field with respect to the c axis is characteristic of an antiferromagnet with the antiferromagnetic axis along or close to the c axis direction.

The observed spontaneous magnetization includes that of a magnetic impurity with Curie temperature at ~150 K, appearing as a step in $\chi'(T)$; this could be assigned to Y_2Ni_{17} which is ferromagnetic with $T_C = 149$ K. The spontaneous magnetization arising at about 150 K has been extrapolated to 5 K yielding ≃12% of the total experimental value, which allows for the estimation of the impurity amount to ≃0.1 wt.%, well below the detection limit in the x-ray diffraction patterns. Thus, the observed weak ferromagnetic component is an intrinsic property of $Y_3Ni_{13}B_2$. The magnetic transition temperature has also been determined on the weak ferromagnetic component, from specific remanence measurement between 5 and 200 K [inset in Fig. 4(a)]; it shows up as a step at 68±2 K, above the Y_2Ni_{17} impurity contribution. This shows that the weak ferromagnetic component develops at the same temperature at which the antiferromagnetic order is established.

The temperature dependence of the reciprocal susceptibility $\chi^{-1}(T)$ of a powder sample above T_N, is plotted in the inset of Fig. 5. The fitting of the linear part (above 120 K) of $\chi^{-1}(T)$ to the Curie-Weiss law yields a positive paramagnetic temperature $\theta_p = 76$ K, consistent with the existence of ferromagnetic correlations in the paramagnetic region. An effective Ni magnetic moment $p_{\text{eff}} = 0.71\ \mu_B$/Ni at. is deduced, close to the values determined for the weak itinerant ferromagnets Y_2Ni_7 and YNI_3 (see Table V).

2. $Y_3Ni_{13-x}Co_xB_2$, $x = 0.5$ and 1

The ac susceptibility of the $Y_3Ni_{12.5}Co_{0.5}B_2$ compound, plotted in Fig. 6, shows two maxima in χ', namely, a broad one centered at 100 K and a sharp one at 86 K, whereas χ'' shows only one peak at 86 K. A small anomaly at 70 K present both in χ' and χ'' is regarded as due to extrinsic effects since no corresponding anomaly is detected in the remanence and disappears with a small applied field (0.1 T). The maxima appear above a background that progressively increases with decreasing temperature below room temperature, to reach a constant value at ~200 K. The temperature dependence of the differential susceptibility $\chi_{\text{diff}\|}$, and $\chi_{\text{diff}\perp}$ at $\mu_0 H_0 = 0.6$ T, derived from the magnetization isotherms plotted in Fig. 7, are drawn in Fig. 8. The thermal variation of the reciprocal susceptibility, plotted in the inset of Fig. 8, can be fitted to the Curie-Weiss law, and one derives an effective 3d magnetic moment $\mu_{\text{eff},3d} = 1.16\mu_B/3d$ at., while $\theta_p = 76$ K, as in $Y_3Ni_{13}B_2$. Similarly to the case of $x = 0$ compound, an applied field $\mu_0 H_0 = 0.6$ T is enough to saturate the weak ferromagnetic component and $\chi_{\text{diff}}(T)$ shows the antiferromagnetic transition cusp at 100 K, a higher temperature than in the Co-free compound. The Néel temperature of the antiferromagnetic ordering is $T_N = 94 \pm 2$ K, while the second transition at which the weak ferromagnetic component sets on is at a critical temperature $T_{\text{WF}} = 86 \pm 2$ K. The temperature dependence of the remanence (see inset in Fig. 6) also shows a steeper increase at 86±2 K, which is the temperature of the lower temperature maximum in $\chi(T)$, indicating the development of a ferromagnetic weak component, as in

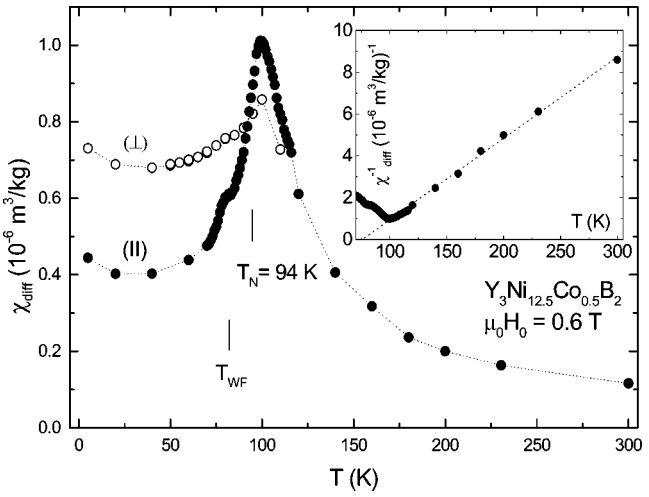

FIG. 8. The temperature dependence of the parallel and perpendicular differential susceptibility of a stacked crystals sample of $Y_3Ni_{12.5}Co_{0.5}B_2$. Inset: the temperature dependence of the reciprocal susceptibility.

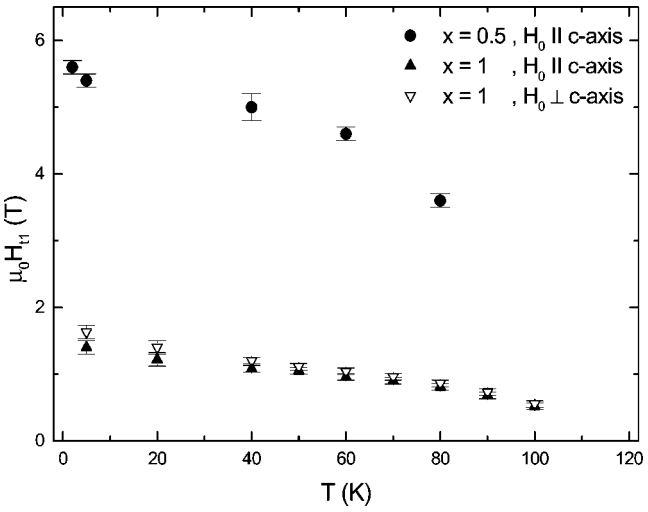

FIG. 9. The temperature dependence of the transition field H_{t1} for $Y_3Ni_{12.5}Co_{0.5}B_2$ and $Y_3Ni_{12}CoB_2$.

$Y_3Ni_{13}B_2$. The effect of the Co inclusion has been, therefore, to decouple the antiferromagnetic and the weak-ferromagnetic transitions.

Similarly to the base compound, an additional ferromagnetic contribution is observed in both the magnetic isotherms and the remanence, with a T_C above room temperature. The secondary phases, $Y(Ni,Co)_4B$ and $Y(Ni,Co)_5$ dilutions, are ferromagnetic above room temperature when more than two Ni atoms are substituted by Co, but no such magnetic transitions were detected in the thermomagnetic measurements in the range 300–1000 K. Therefore, the secondary phases detected by x-ray diffraction should be the corresponding Ni-rich dilutions, which are paramagnetic. It may be conjectured that the parasitic ferromagnetism with T_C above room temperature is due to ferromagnetic Co clusters in the sample. Their presence may be associated with composition heterogeneities due to local fluctuations in cobalt concentration. The relevant magnetic data relative to $Y_3Ni_{12.5}Co_{0.5}B_2$ are given in Table IV.

Below 100 K, the magnetization curves show that a field-induced process takes place [see Figs. 7(a) and 7(b)]. The transition is better observed in the $M(H)$ curve with the applied field parallel to the c axis than in the case of the perpendicular applied field. Measurements up to 10 T at 2 and 5 K show the transition at μ_0H_t=5.6 T, taken at the inflexion point, for H_0 both parallel and perpendicular to the c axis. $H_t(T)$ derived from the $M(H)$ curves with $H_0 \| c$ axis, plotted in Fig. 9, decreases when temperature increases. The transition is accompanied by a field hysteresis, which can be observed up to 40 K.

The temperature dependence of the ac susceptibility of $Y_3Ni_{12}CoB_2$, plotted in Fig. 10, shows two peaks in $\chi'(T)$ at 92 and 110 K, but only the lower temperature one has a corresponding peak in $\chi''(T)$. As for the x=0.5 compound, this behavior is consistent with a transition from paramagnetism to antiferromagnetic order near ~110 K, with the lower temperature peak corresponding to the onset of the weak ferromagnetic component at T_{WF}=92±2 K. In fact, heat capacity measurements showed a peak at 106 K due to the antiferromagnetic long range ordering, while no anomalous feature could be observed at 92 K;[37] thus, we take T_N =106±2 K. The antiferromagnetic transition is also revealed by a cusp in the $M(T)$ curves for $\mu_0H_0<2$ T, i.e., below the applied field range of values which induce the transition to ferromagnetic behavior, corresponding to the jump observed in the magnetization isotherms for $T<110$ K (Fig. 11). On the other hand the WF component is quenched by a moderate applied field. Thus, the same type of temperature-induced magnetic transitions when lowering the temperature, first from paramagnetism to antiferromagnetic order at T_N, and a subsequent one, which presents a weak ferromagnetic component, are observed, as in the $Y_3Ni_{12.5}Co_{0.5}B_2$ compound at zero field. The further increase in the Co content from 0.5 to 1.0 atom per formula unit has the effect of shifting the transition temperature by a few degrees.

The magnetization does not reach saturation in fields up to 5 T, see Fig. 11. Since in the paramagnetic temperature range, the $M(H)$ curves show a spontaneous magnetization

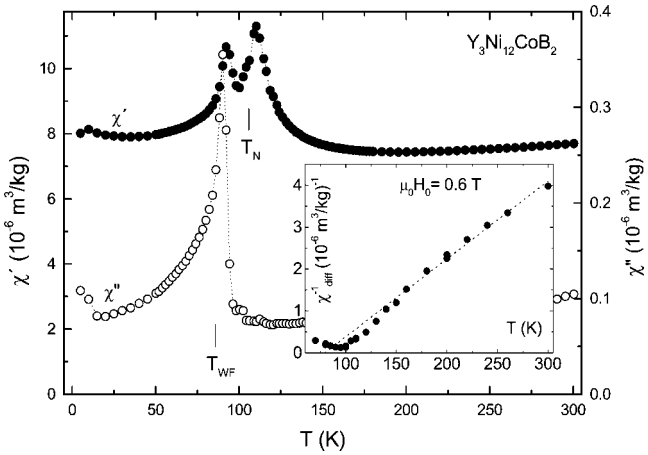

FIG. 10. The temperature dependence of the ac susceptibility of $Y_3Ni_{12}CoB_2$. Inset: the temperature dependence of the reciprocal susceptibility.

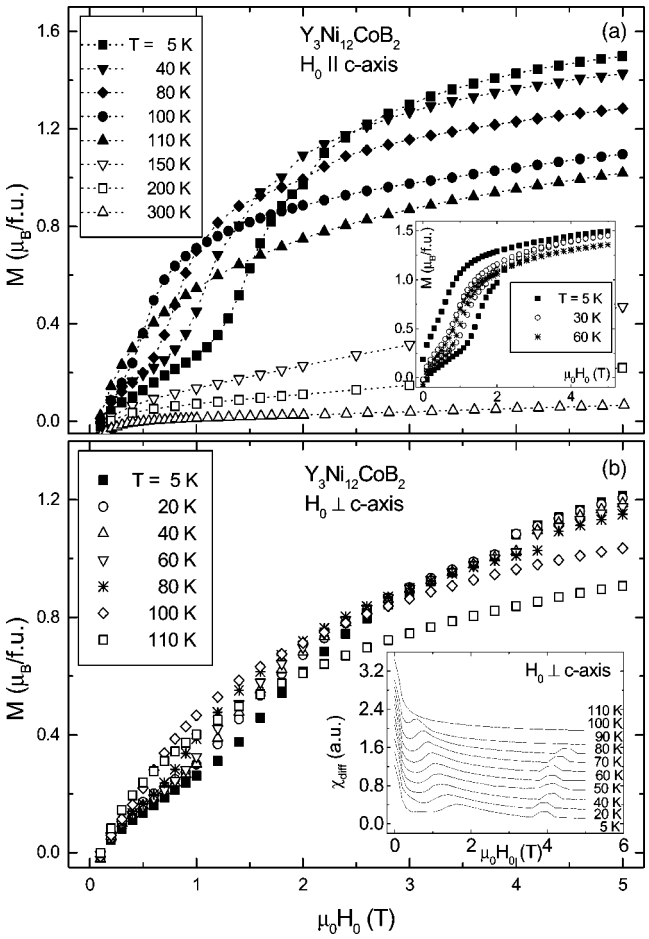

FIG. 11. The magnetization isotherms of the $Y_3Ni_{12}CoB_2$ compound, with $H_0 \| c$ axis (a) and $H_0 \perp c$ axis (b). Inset in (a): the field hysteresis at some temperatures. Inset in (b): The field dependence of the differential susceptibility.

of 0.83 A m^2/kg at 300 K, which marks the presence of a ferromagnetic impurity, the magnetization isotherms in Fig. 11 have been corrected by substracting the impurity contribution approximated by its value at 300 K. The values of the magnetization and superimposed susceptibility of a stacked crystal sample of $Y_3Ni_{11}CoB_2$ are given in Table IV.

The field-induced transition AF to F is accompanied by a hysteresis, as observed below 110 K (Fig. 11), and takes place at lower fields than in the case of $Y_3Ni_{12.5}Co_{0.5}B_2$. The hysteresis area and the transition field decrease when temperature increases, see the inset of Figs. 11(a) and 9, respectively. The hysteresis width at the transition is of 1.1 T at 5 K, decreases to 0.13 T at 60 K and disappears at 80 K. The field derivative of the magnetization curves with $H_0 \perp c$ axis shows a second maximum at field values higher than H_{t1}, see the inset in Fig. 11(b). The critical field of this transition H_{t2} increases with temperature, opposite to the temperature dependence of H_{t1}, which suggests different underlying physical mechanisms.

3. $Y_3Ni_{13-x}Co_xB_2$, $2 \leqslant x \leqslant 5$

These compounds are ferromagnetic, as evidenced by the magnetization isotherms measured on powder samples at

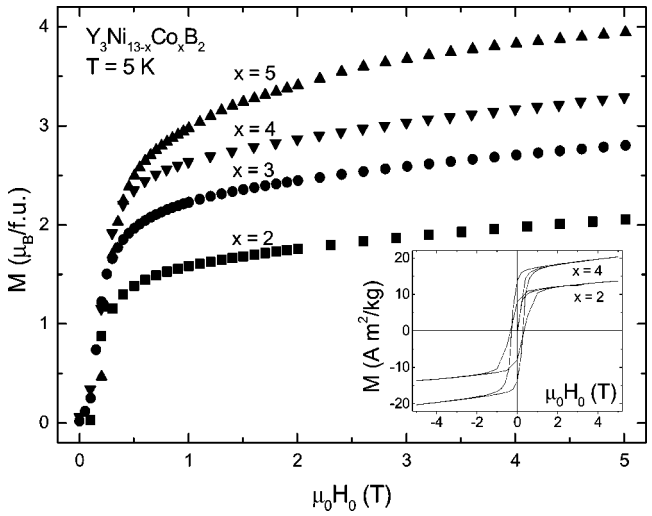

FIG. 12. The magnetization isotherms at 5 K of the $Y_3Ni_{13-x}Co_xB_2$ compounds, with $2 \leqslant x \leqslant 5$. Inset: the hysteresis loops at 5 K for the compounds with $x=2$ and 4.

5 K and plotted in Fig. 12. The T_C values, given in Table VI, have been determined as the peak position on the $\chi'(T)$ curves, plotted in Fig. 13.

In the paramagnetic phase, the $M(H)$ dependence is linear, except in the low-field region ($\leqslant 0.5$ T), where it deviates from linearity and shows the presence of a parasitic spontaneous magnetization. The impurity phase has been estimated to amount up to 2 A m^2/kg at RT, by linear extrapolation of the high field part of the $M(H)$ curves to zero field. This value was taken as an approximate contribution of the ferromagnetic impurities with T_C higher than RT and subtracted from the saturation magnetization derived by fitting the magnetization isotherms at $\mu_0 H_0 > 2.5$ T to the equation $M(H) = M_S(1 - b/H^2) + \chi_0 H$; the corrected M_S values and those of the superimposed susceptibility χ_0 at 5 K, are also listed in Table VI. The saturation magnetization and the Curie temperature of these compounds increase linearly with the Co content within the uncertainty due to cobalt concentration variations,[37,38] which suggests that in this composition range the contribution of the Ni sublattice to the ferromagnetic moment might be negligible, and that the Co moment plays a dominant role in the magnetic ordering transition.

From the analysis of the relative intensities of selected pairs of peaks observed in the x-ray diffraction patterns of

TABLE VI. The Curie temperature T_C, spontaneous magnetization at 5 K M_S, the mean Co moment μ_{Co}, the mean 3d atom moment μ_{3d}, and the superimposed susceptibility χ_0, of $Y_3Ni_{13-x}Co_xB_2$ compounds with $2 \leqslant x \leqslant 5$.

x, Co	T_C (±2 K)	M_S at 5 K (μ_B/f.u.)	μ_{Co} at 5 K (μ_B/Co at.)	μ_{3d} at 5 K (μ_B/3d at.)	χ_0 at 5 K (10^{-6} m^3/kg)
2.0	146	1.72	0.86	0.13	0.47
3.0	170	2.39	0.80	0.18	0.59
4.0	201	2.75	0.69	0.21	0.76
5.0	241	3.63	0.73	0.28	0.57

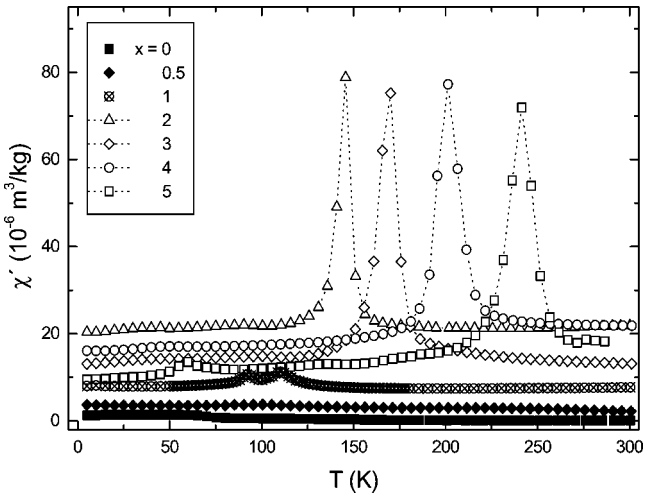

FIG. 13. The temperature dependence of the real part of the ac susceptibility, for $x \leqslant 5$.

magnetic field-oriented powders, with respect to those of random powders, we derive that the easy magnetization direction lays in the basal plane, in $Y_3Ni_{13-x}Co_xB_2$, with $2 \leqslant x \leqslant 5$. The compounds also exhibit significant intrinsic coercivity at 5 K, as proven by the hysteresis loops measured on large grains fixed in grease, attaining values of, e.g., 0.34 T for $x=2$ and 0.29 T for $x=4$, see the inset of Fig. 12.

IV. DISCUSSION

A. Weak itinerant magnetism in $Y_3Ni_{13-x}Co_xB_2$, with $x \leqslant 1$

In the $Y_3Ni_{13-x}Co_xB_2$ series, the present susceptibility and magnetization data indicate the onset of antiferromagnetic ordering below a Néel temperature of $T_N=68$, 94, and 106 K for $x=0$, 0.5, and 1, respectively. A weak ferromagnetic component also develops at T_N for $x=0$, and below T_N for $x=0.5$ and 1, in evidence of a noncompensated 3*d* magnetic structure. Since in crystal structures with inversion center, as is the case of the $Nd_3Ni_{13}B_2$ one, canted antiferromagnetism is not allowed,[39] the ferromagnetic component may arise as a result of a complex antiferromagnetic-type ordering with more than two sublattices. The coexistence of antiferromagnetism and ferromagnetism in itinerant electron systems has been predicted by Moriya and Usami.[40,41] The sequence of transitions we observe for the $x=0.5$ and $x=1$ compounds, i.e., an AF phase below T_N and a WF phase below $T_{WF} < T_N$ coexisting with the AF phase down to the lowest temperature, may be related to their case II-2; although in that case the AF phase is shown to disappear at a finite temperature, this can be as low as 0 K, as in the present case.

The cusp observed in the temperature dependence of χ', at T_N, shows that the AF correlations establish as the 3*d* electron system approaches the spin ordering temperature. Indeed, the reciprocal susceptibility at high temperature for $x=0, 0.5$, and 1 has a positive θ_p, indicating ferromagnetic correlations, while the cusp and subsequent decrease of the susceptibility down to the long-range ordering transition at T_N, and shape of the χ_{diff} curves, once that the weak ferromagnetic component is saturated, are unambiguously characteristic of antiferromagnetic behavior. On the other hand, the cusp does not appear in the $(2 \leqslant x \leqslant 5)$ compounds, when the substitution of Ni by Co enhances the ferromagnetic interactions.

The application of a moderate applied field shifts the transition temperature T_N to lower temperatures for $x=0.5$ and 1, as could be expected for antiferromagnets. In contrast, for $x=0$ the shift is to slightly higher temperature which is an unexpected result. The different behavior may be relateed to the fact that for $x=0$ the WF component appears simultaneously with the AF ordering at T_N, while for $x=0.5$ and 1 only the AF component arises at T_N and thus the conventional behavior takes place. A similar increase in T_N with the applied field was observed in the itinerant electron La_2Ni_7 (with Ce_2Ni_7-type structure), which was found to order antiferromagnetically at $T_N=54$ K.[42,43,53]

In $Y_3Ni_{13}B_2$ the values of the differential susceptibility at the Néel temperature, at 0.6 T, are different by $\sim$20% between the measurements with the applied field parallel and perpendicular, respectively, to the *c* axis, which reveals the anisotropy of the compound (Fig. 5). At low substitution, the Ni sublattice still holds its own basically antiferromagnetic phase. The paramagnetic susceptibility for $x=0.5$ and 1 may be analyzed as emerging from the contributions of the Ni atoms, contributing to the effective magnetic moment $p_{eff,Ni}=0.71\ \mu_B$, as deduced from the $x=0$ compound, and that of Co atoms by a quantity to be deduced from the experimental values for p_{eff} given in Table IV. The result for $x=0.5$ and $x=1$ is $p_{eff,Co}=4.8$ and $5.6\mu_B$/at., respectively. These values are higher than $\approx 4\mu_B$/Co at. in ACo_2 (A=Y, Lu, Sc, and Hf)[44] and close to $5.45\mu_B$ found for $YCo_{2.5}Ni_{2.5}$.[45] In spin fluctuation systems, values higher than the Co^{2+} effective moment for quenched orbital moment ($3.87\mu_B$), may be attributed to an orbital contribution.

One can estimate the degree of itinerancy of the 3*d* magnetic moments in the $Y_3Ni_{13-x}Co_xB_2$ compounds from the magnitude of the Rhodes-Wohlfarth parameter $r=q_c/q_s$ (the ratio between the number of magnetic carriers in the paramagnetic phase q_c and that at saturation q_s).[46] In the case of the base compound, using the value $\mu_{Ni}=0.034\mu_B$ at 10 T and 2 K, as a lower limit of the mean nickel moment, and the value $p_{eff}=0.71\mu_B$/Ni at. derived from the Curie constant, one obtains $r \lesssim 6.8$. In the case of the $x=0.5$ compound, using the 3*d* moment value determined at 2 K and 10 T, $\mu_{3d}=0.083\mu_B$ and the value of $p_{eff}=1.16\mu_B/3d$ at., then it results $r \lesssim 6.4$. Finally, for $x=1$, where magnetic saturation is almost reached at 5 K and 5 T, $\mu_{3d}=0.12\mu_B$ and the effective moment $p_{eff} \approx 1.7\mu_B$ produces $r \approx 8$. Although the first values are overestimated and the last one may be affected by some error due to the narrow temperature range considered (160–300 K), they certainly point to a high degree of itinerancy of the 3*d* magnetic moments in the Ni-rich $Y_3Ni_{13-x}Co_xB_2$ compounds, following the criterion of Ref. 46. This is in agreement with the *r* values determined in the structurally related $Y_3Ni_{11-x}Co_xB_4$ (Ref. 47) and $YNi_{4-x}Co_xB$ (Ref. 48) in the nickel-rich composition range; in these series the *r* parameter takes values from 6.9 for $x=5$ to 3.8 for $x=11$, and from 5.3 for $x=1$ to 2.0 for $x=4$, respectively. Although the magnetic measurements yield $\mu_{3d} \approx 0.2\mu_B$ for the mean 3*d* magnetic moment in

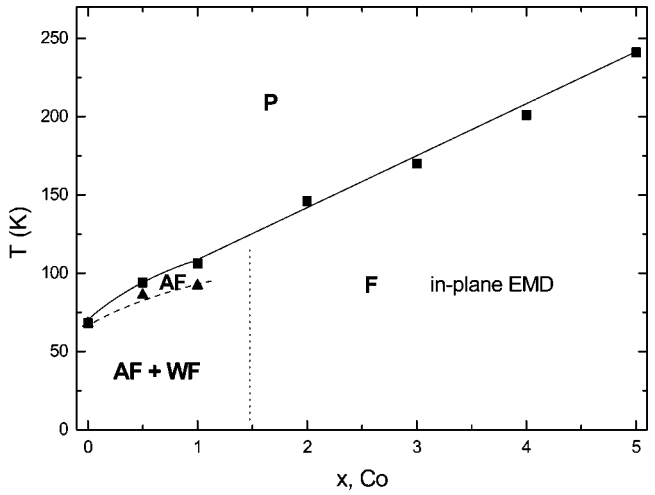

FIG. 14. The *T*-*x* magnetic phase diagram of the $Y_3Ni_{13-x}Co_xB_2$ compounds, $x \leqslant 5$, in zero applied field.

$Y_3Ni_{10}Co_3B_2$, neutron-diffraction experiments did not reveal a magnetic contribution within the experimental resolution. This points again to a highly delocalized character of the 3*d* moments in $Y_3Ni_{13-x}Co_xB_2$.

B. The *T*-*x* phase diagram

The magnetic phase diagram of the $Y_3Ni_{13-x}Co_xB_2$ compounds $x \leqslant 5$ derived from the experimental data in zero applied field, is plotted in Fig. 14. Below the magnetic order temperature, the region between $x=0$ and 1 corresponds to an AF phase, with a WF component below T_{WF}, the latter resulting from uncompensated 3*d* magnetic moments. Since the 3*d* metal atoms are distributed on three crystallographically different lattice sites in the $Nd_3Ni_{13}B_2$-type cell, one may expect a complex AF structure. The magnetization isotherms of the $x=0.5$ and 1 compounds (see Figs. 7 and 11) show that, at a given temperature, a field-induced transition from antiferromagnetic to ferromagnetic phase occurs at a critical field H_{t1}. The values of H_{t1} for the applied field parallel and perpendicular to the *c* axis are indiscernible. From the composition dependence of H_{t1}, i.e., it increases with decreasing x ($H_{t1}=1.6$ T for $x=1$ and 5.6 T for $x=0.5$, at 5 K) one may expect the transition to appear also in the base compound; however, since we do not observe any transition up to 10 T [see the inset in Fig. 4(b)] we conjecture that it should appear at a higher field. The magnetization approaches faster to saturation above H_{t1} as x increases; therefore, we conclude that the net *F* component is enforced by the cobalt substitution for nickel.

In zero applied field, the change from the AF+WF phase to the *F* phase takes place in a composition range between $x=1$ and 2, marked by the dotted line on the phase diagram. For $(2 \leqslant x \leqslant 5)$ the transition is from a paramagnetic to a ferromagnetic phase below the Curie temperature represented by the thick line in Fig. 14 and the compounds show in-plane anisotropy, as could be deduced from the x-ray diffraction experiments on oriented powders. On the grounds of the structural relationship between the 1:5 and the 3:13:2 cells, the in-plane EMD in $Y_3Ni_{13-x}Co_xB_2$ for $2 \leqslant x \leqslant 5$ correlates well with both the proposed substitution scheme, i.e., Co is presumed to preferentially substitute Ni at the 3*g* and 6*i* sites for $x \leqslant 5$, and the site contribution to anisotropy in YCo_5.[49] According to Ref. 49 cobalt at the 2*c* sites has a large and positive contribution to the second order anisotropy constant K_1 and cobalt at the 3*g* sites has a small and negative contribution to K_1. Thus, one may expect that cobalt at the 3*g* and 6*i* sites in 3:13:2 contributes to in-plane anisotropy, as experimentally observed.

The step in the magnetization curve [peak in $\chi_{diff}(H)$] at applied field values ~4 T in $Y_3Ni_{12}CoB_2$, see Fig. 11, may be related to itinerant 3*d* electron metamagnetism (IEM). Indeed, the critical field H_{t2} increases with the temperature, as expected for an itinerant metamagnet.[16] The critical fields of IEM systems range from tens of T to a few T,[15,16,18,50] and it can take place as a transition from a paramagnetic to a ferromagnetic phase,[51] as well as from a low moment to high moment ferromagnetic phase,[52] as may be the present case. IEM of Co sites in the $Y_3Ni_{12}CoB_2$ compound would be rather unusual for such a low Co concentration; on the other hand, IEM transitions at the Ni sites in the present compound are more likely to occur in view of the strong anisotropy in the 3*d* moment, see Table IV. Also, IEM of Ni at low critical field was observed in the hexagonal La_2Ni_7.[53] The temperature dependence of the critical field can be fitted to a $H_{t2}(T)=H_{t2}(0)+\alpha T^2$ law, yielding $H_{t2}(0)=3.90$ T and $\alpha=6\times10^{-5}$ T/K^2. The present value of α is about 20 times smaller than that of a low critical field metamagnet $Lu(Co_{0.91}Ga_{0.09})_2$,[54] which might be due to the different type of metamagnetic transition (low moment to high moment ferromagnets) with respect to that of $Lu(Co_{0.91}Ga_{0.09})_2$ (paramagnet to ferromagnet).

Previously, the large intrinsic coercivity observed in the $R(Co,Ni)_5$ series for intermediate Co contents,[55] has been attributed to domain wall pinning at lattice sites where local variations in the magnetic anisotropy energy occurs. It has experimentally been proven that such variations in anisotropy and exchange are promoted by the occurrence of high and low Co moment sites, actually magnetic heterogeneities which act as domain wall pinning centers in the crystallographically ordered lattice.[11–13] In view of the close structural relationship between the 1:5 and 3:13:2 series, we suggest that a similar mechanism, i.e., the development of a magnetically heterogeneous system with high and low 3*d* moment sites when Co replaces Ni in $Y_3Ni_{13-x}Co_xB_2$ should be responsible for the observed increase in the temperature domain of magnetic irreversibility and the intrinsic coercivity, for $2 \leqslant x \leqslant 5$.

C. The magnetic behavior of the (Ni,Co) sublattice in $Y_3Ni_{13-x}Co_xB_2$ and related compounds

This is a first report on the antiferromagnetic ordering of $Y_3Ni_{13}B_2$ and its evolution in the $Y_3Ni_{13-x}Co_xB_2$ series for $x \leqslant 1$. Due to the high degree of delocalization of the 3*d* moments, a proper approach for the description of the AF state should be based on itinerant electron theories of antiferromagnetism. An estimation of the change in the magnetic

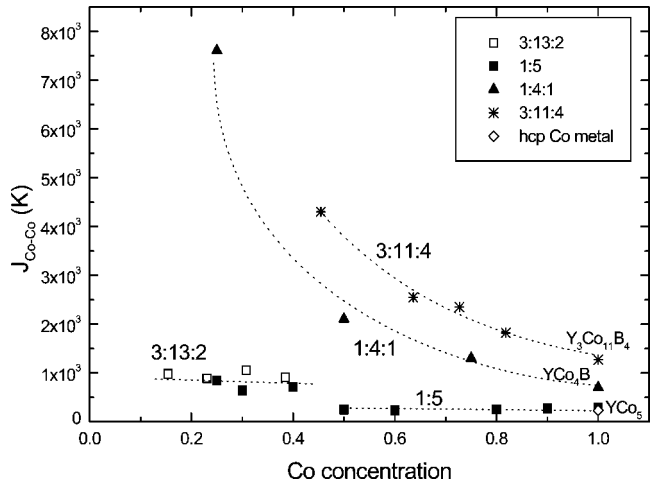

FIG. 15. The exchange parameter J_{CoCo} versus Co concentration in the $Y_3(Ni,Co)_{13}B_2$, $Y(Ni,Co)_4B$, $Y_3(Ni,Co)_{11}B_4$, and $Y(Ni,Co)_5$ series.

state of the compounds in this composition range may be obtained in the mean-field approximation by observing that the perpendicular differential susceptibility takes the values 0.39×10^{-6}, 0.73×10^{-6}, and 1.69×10^{-6} m^3/kg at 5 K for $x=0,0.5$, and 1, respectively. This increase in $\chi_{\mathrm{diff},\perp}$ with the Co content is consistent with a decrease in the AF molecular field constant in the mean-field approximation.

The saturation magnetization of the compounds with $2\leqslant x\leqslant5$ linearly increases with the Curie temperature, in the limit of the experimental errors, in agreement with a rigid band model. Under the assumption that a 3*d* magnetic moment is present only at the Co sites and therefore, the Ni magnetic moment may be neglected, one determines the mean cobalt moment μ_{Co} given in Table VI. The so-obtained cobalt moment is independent of the concentration, with $\mu_{\mathrm{Co}}=0.78\pm0.08$ μ_B/Co at., in the studied composition range. A mean-field analysis of the Co-Co exchange interaction can be carried out under the assumption that the rigid band model is a valid approximation and assuming that Ni is nonmagnetic in the above systems. Then, the Co-Co exchange parameter $J_{\mathrm{Co\text{-}Co}}$ may be expressed as $J_{\mathrm{Co\text{-}Co}}=6T_C/(\xi z\mu_{3d}^2)$ (in K), where we have introduced the cobalt concentration ξ in order to account for the variation in the number of Co-Co interactions with the different Co contents and ξz is the average number of Co atoms near neighbors to a Co atom.[56,57] In $Y_3Ni_{13-x}Co_xB_2$, with $2\leqslant x\leqslant5$ we obtain the values $J_{\mathrm{Co\text{-}Co}}=980$, 887, 1056, and 908 K, for $x=2$, 3, 4, and 5, respectively. We apply the same procedure to the related $Y(Ni,Co)_5$, $Y(Ni,Co)_4B$, and $Y_3(Ni,Co)_{11}B_4$ series, for which the Curie temperature and magnetization data are reported in the literature. The Co concentration dependence of $J_{\mathrm{Co\text{-}Co}}$ is displayed in Fig. 15. The representation sheds a light on the range of ξ values, i.e., range of compositions, in which the behavior of the (Ni,Co) sublattice in $R_{m+n}T_{5m+3n}B_{2n}$ compounds either exhibits strong ferromagnetism or is dominated by magnetic instabilities and spin fluctuations.

In the case of the $YNi_{5-x}Co_x$ series, the exchange parameter takes values close to that in Co metal (a classic strong ferromagnet), $J_{\mathrm{Co\text{-}Co}}=230$ K, and is almost insensitive to both Ni substitution and the change in the local environment for a cobalt concentration decreasing to about 40–50%. In this composition range the (Ni,Co) sublattice preserves its strong ferromagnetic character. For a Co concentration less than 50%, the $J_{\mathrm{Co\text{-}Co}}$ increases, which may be related to the onset of magnetic instabilities and increasing effect of spin fluctuation. By similarity, the data for the 3:13:2 series, situated close to those of the Ni-rich 1:5 compounds (recall that there are two 1:5 slabs in the 3:13:2 cell), suggest an unstable magnetic behavior dominated by spin fluctuations, for $2\leqslant x\leqslant5$, consistent with the high Co paramagnetic moments deduced in Sec. IV A of this discusion. In the case of the $YNi_{4-x}Co_xB$ and $Y_3Ni_{11-x}Co_xB_4$ series, the high, nonphysical values found for $J_{\mathrm{Co\text{-}Co}}(c)$ in the mean-field model suggest that spin fluctuations have a significant contribution to the magnetic behavior of the (Ni,Co) sublattice, except in a narrow composition range, in the Co-rich region.

Under the assumption of a unique 3*d* band and delocalized magnetic moments, as supported by preliminary data of neutron diffraction experiments, one derives from the experimental M_S values the mean 3*d* moment μ_{3d} also listed in Table VI. The μ_{3d} values increase when cobalt substitutes for Ni, which may be accounted for by a gradual depletion mechanism of the 3*d* minority spin subband and an evolution of the density of states at the Fermi level. Actually, on the grounds of the metallurgically inhomogeneous nature of the system, which determines an inhomogeneous magnetic estate, one may assume that both described mechanisms may be present.

V. CONCLUSIONS

The $Y_3Ni_{13-x}Co_xB_2$ series of compounds with $Nd_3Ni_{13}B_2$-type structure has been synthesized for a cobalt content $x\leqslant5$. The magnetic properties emerge from the (Ni,Co) sublattice and the large values of the Rhodes-Wohlfarth parameter, estimated for the $x=0$, 0.5, and 1, support a high degree of itinerancy of the 3*d* magnetic moments. The susceptibility and magnetization data evidence for an antiferromagnetic phase for $x\leqslant1$, in zero applied field. Based on present results we suggest that the weak ferromagnetic component observed below T_{WF} is an intrinsic property of the magnetic structure of these compounds. The uncompensated AF order is favored by the presence of three different 3*d* lattice sites, which may have different magnetic contributions. The intrinsic WF component increases with increasing the cobalt content from $x=0$ to $x=1$ and for $x\geqslant2$ the compounds are ferromagnetic. We mention that, to our knowledge, the Ce_2Ni_7-type La_2Ni_7,[53] is the only other antiferromagnetically-ordered metallic Ni compound known so far, in which only Ni atoms bear a magnetic moment.[42,46] The compounds with $0<x\leqslant1$ undergo a field-induced transition to a state with an enforced net ferromagnetic component, at a critical field H_{t1}, which decreases when either the Co content or temperature increase. This transition is observed up to a temperature higher than T_N, but lower than that of the AF peak. The occurrence of another field-induced transition at a field H_{t2} larger than H_{t1}, as observed for x

$=1$, could be due to itinerant electron metamagnetic transitions.

The remarkable evolution in the 3*d* sublattice magnetic behavior for x increasing from 0 to 1 should be ascribed only to the change in the 3*d* electron concentration in the system, since the structural effect of cobalt substitution for nickel is rather negligible, for $x \leqslant 1$. The compounds in the composition range $2 \leqslant x \leqslant 5$ are ferromagnetic and their Curie temperature and spontaneous magnetization increase with the cobalt content. An analysis of the Co-Co exchange parameter as a function of the Co concentration shows that the behavior in the presently studied 3:13:2 series is similar to that determined for the related Ni-rich 1:5, whereas the 1:4:1 and 3:11:4 series show nonphysical values of $J_{\text{Co-Co}}$. The deviation from the strong (Stoner) ferromagnetism is attributed to the effect of spin fluctuations on the magnetic properties of these compounds.

ACKNOWLEDGMENTS

This work was supported under a CICYT MAT 02/00166 grant. V. Pop thanks the University Joseph Fourier (Grenoble, France) for a grant of "Professeur invité" and the Laboratoire de Magnétisme Louis Néel of the CNRS in Grenoble for the research facilities. M. Castro is acknowledged for the heat capacity measurements of the $x=1$ sample.

*Also at: National Institute of Materials Physics POBox MG-7, 76900 Bucharest, Romania.

†Also at: Laboratoire Louis Néel, CNRS, Associé 'a l'Université Joseph Fourier (Grenoble) et l'Institut National Polytechnique de Grenoble, BP 166 X, 38042 Grenoble cedex 9, France.

[1] E. Parthand B. Chabot, in *Handbook on the Physics and Chemistry of Rare Earths*, edited by K. A. Gschneidner, Jr. and L. Eyring (Elsevier Science, Amsterdam, 1984), Vol. 6, p. 113.

[2] K. H. J. Buschow, in *Ferromagnetic Materials*, edited by E. P. Wohlfarth and K. H. J. Buschow (Elsevier, Amsterdam, 1988), Vol. 4, p. 1.

[3] K. J. Strnat and R. M. W. Strnat, J. Magn. Magn. Mater. **100**, 38 (1991)

[4] H.-S. Li and J. M. D. Coey, in *Handbook of Magnetic Materials* (Ref. 2), Vol. 6, p. 1.

[5] D. Gignoux, F. Givord, R. Lemaire, and F. Tasset, J. Less-Common Met. **94**, 1 (1983).

[6] R. Ballou, V. M. T. S. Barthem, and D. Gignoux, Physica B & C **149**, 340 (1988).

[7] J. J. M. Franse and R. J. Radwanski, in *Handbook of Magnetic Materials* (Ref. 2), Vol. 7, p. 307.

[8] N. M. Hong, T. Holubar, G. Hilscher, M. Vybornov, and P. Rogl, IEEE Trans. Magn. **30**, 4966 (1994).

[9] N. M. Hong, H. Michor, M. Vybornov, T. Holubar, P. Hundegger, W. Perthold, G. Hilscher, and P. Rogl, Physica C **227**, 85 (1994).

[10] K. H. Müller, G. Fuchs, S. L. Drechsler, and V. N. Narozhnyi, in *Handbook of Magnetic Materials* (Ref. 2), Vol. 14, p. 199.

[11] H. Oesterreicher, F. T. Parker, and M. Misroch, Phys. Rev. B **18**, 480 (1978).

[12] A. S. Ermolenko, A. Z. Menshikov, and Yu. A. Dorofeev, Phys. Status Solidi A **54**, K113 (1979).

[13] A. V. Korolyov, N. V. Mushnikov, V. S. Gaviko, Ye. G. Gerasimov, A. S. Ermolenko, and V. I. Chrabrov, J. Magn. Magn. Mater. **140–144**, 859 (1995).

[14] D. Givord, J. Laforest, R. Lemaire, and Q. Lu, J. Magn. Magn. Mater. **31–34**, 191 (1983).

[15] M. I. Bartashevich, T. Goto, A. V. Korolyov, and A. S. Ermolenko, J. Magn. Magn. Mater. **163**, 199 (1996).

[16] T. Goto, M. I. Bartashevich, A. V. Korolyov, and A. S. Ermolenko, Physica B **246–247**, 149 (1998).

[17] H. Yamada, K. Terao, F. Ishikawa, M. Yamaguchi, and T. Goto, J. Phys.: Condens. Matter **11**, 483 (1999).

[18] F. Ishikawa, I. Yamamoto, I. Umehara, M. Yamaguchi, M. I. Bartashevich, H. Mitamura, T. Goto, and H. Yamada, Physica B **328**, 386 (2003).

[19] Yu. B. Kuz'ma and N. S. Bilonishko, Dopov. Akad. Nauk. Ukr. RSR, Ser. A: Fiz.-Mat. Tekh. Nauki **10**, 87 (1981).

[20] Yu. B. Kuz'ma, N. S. Bilonishko, N. F. Chaban, and G. V. Chernyak, J. Less-Common Met. **90**, 217 (1983).

[21] P. Rogl, in *Handbook on the Physics and Chemistry of Rare Earths*, edited by K. A. Gschneidner, Jr. and L. Eyring (Elsevier, Amsterdam, 1984), Vol. 6, p. 470.

[22] N. M. Hong, N. P. Thuy, G. Schaudy, T. Holubar, G. Hilscher, and J. J. M. Franse, J. Appl. Phys. **73**, 5698 (1993).

[23] Y. Chen, Q. L. Liu, J. K. Liang, X. L. Chen, B. G. Shen, and F. Huang, Appl. Phys. Lett. **74**, 856 (1999).

[24] Y. Chen, X. Li, X. L. Chen, J. K. Liang, G. H. Rao, B. G. Shen, Q. L. Liu, L. P. Jin, and M. Z. Wang, Chem. Mater. **12**, 1240 (2000).

[25] Y. Chen, J. K. Liang, X. L. Chen, and Q. L. Liu, J. Alloys Compd. **289**, 96 (1999).

[26] Y. Chen, J. K. Liang, X. L. Chen, and Q. L. Liu, J. Alloys Compd. **296**, L1 (2000).

[27] Y. Chen, X. Li, X. L. Chen, J. K. Liang, G. H. Rao, and Q. L. Liu, J. Alloys Compd. **305**, 216 (2000).

[28] J. Rodriguez-Carvajal, program FullProf.2k, Version 1.9c, Laboratoire Leon Brillouin, Saclay, France.

[29] J. H. Wernick and S. Geller, J. Appl. Crystallogr. **12**, 662 (1959).

[30] Y. C. Chuang, C. H. Wu, and Y. C. Chang, J. Less-Common Met. **84**, 201 (1982).

[31] K. Uebayashi, K. Terao, and H. Yamada, J. Alloys Compd. **346**, 47 (2002).

[32] D. Gignoux, R. Lemaire, and P. Molho, J. Magn. Magn. Mater. **21**, 119 (1980).

[33] I. S. Dubenko, R. Z. Levitin, A. S. Markosyan, A. B. Petropavlosky, and V. V. Snegirev, J. Magn. Magn. Mater. **90–91**, 715 (1990).

[34] R. Nakabayashi, Y. Tazuke, and S. Murayama, J. Phys. Soc. Jpn. **61**, 774 (1992).

[35] D. Gignoux, R. Lemaire, P. Molho, and F. Tasset, J. Magn. Magn. Mater. **21**, 307 (1980).

[36] L. J. de Jongh and A. R. Miedema, Adv. Phys. **23**, 1 (1974).
[37] M. Castro (private communication).
[38] D. Wagner and E. P. Wohlfarth, J. Phys. F: Met. Phys. **9**, 717 (1979).
[39] J. S. Smart, *Effective Field Theories of Magnetism* (Saunders, Philadelphia, 1966), p. 101.
[40] T. Moriya and K. Usami, Solid State Commun. **23**, 935 (1977).
[41] T. Moriya, *Spin Fluctuations in Itinerant Electron Magnetism* (Springer-Verlag, Berlin, 1985).
[42] K. H. J. Buschow, J. Magn. Magn. Mater. **40**, 224 (1983).
[43] Y. Tazuke, M. Abe, and S. Funahashi, Physica B **237–238**, 559 (1997).
[44] E. Burzo, E. Gratz, and V. Pop, J. Magn. Magn. Mater. **123**, 159 (1993).
[45] P. Gerard, Ph.D. thesis, Université Joseph Fourier, Grenoble, 1992.
[46] P. Rhodes and E. P. Wohlfarth, Proc. R. Soc. London, Ser. A **273**, 247 (1963).
[47] E. Burzo, V. Pop, and R. Ballou, J. Magn. Magn. Mater. **157–158**, 631 (1996).
[48] E. Burzo, V. Pop, M. Mihet, and I. Lupsa, Balkan Phys. Lett. **3**, 60 (1995).
[49] R. L. Streever, Phys. Rev. B **19**, 2704 (1979).
[50] H. Michor, M. El-Hagary, M. D. Mea, M. W. Pieper, M. Reissner, G. Hilscher, S. Khmelevskyi, P. Mohn, G. Schneider, G. Giester, and P. Rogl, Phys. Rev. B **69**, 081404 (2004).
[51] E. P. Wohlfarth and P. Rhodes, Philos. Mag. **7**, 1817 (1962).
[52] M. Shimizu, J. Phys. (Paris) **43**, 155 (1982).
[53] M. Fukase, Y. Takuze, H. Mitumura, T. Goto, and T. Sato, Mater. Trans., JIM **41**, 1046 (2000).
[54] K. Murata, K. Fukamichi, T. Sakakibara, T. Goto, and H. A. Katori, J. Phys.: Condens. Matter **5**, 2583 (1993).
[55] K. H. J. Buschow and M. Brouha, J. Appl. Phys. **47**, 1653 (1976).
[56] J. F. Herbst, Rev. Mod. Phys. **63**, 819 (1991).
[57] D. Givord and D. Courtois, J. Magn. Magn. Mater. **196–197**, 684 (1999).